Fukumoto, M., Kurisu, S., Yamada, T., Takenawa, T.	α-Actinin 4 enhances colorectal cancer cell invasion by suppressing focal adhesion maturation.	Plos One	In press		2014
Okamoto, N., Suzuki, H., Kawahara, K., Honda, K., Miura, N., Hirashima, T., Tamiya, M., Morishita, N., Shiroyama, T., Tanaka, A., Tani, E., Hamaguchi, M., Kitani, M., Yamada, T., Kawase, I.	The alternatively spliced actinin-4 variant as a prognostic marker for metastasis in small-cell lung cancer.	Anticancer Res.	35	1663-7	2015
Kamita, M., Mori, T., Sakai, Y., Ito, S., Gomi, M., Miyamoto, Y., Harada, A., Niida, S., Yamada, T., Watanabe, K., Ono, M.	Proteomic analysis of ligamentum flavum from patients with lumbar spinal stenosis.	Proteomics	In press		2015
Watanabe, T., Ueno, H., Watabe, Y., Hiraoka, N., Morizane, C., Itami, J., Okusaka, T., Miura, N., Kakizaki, T., Kakuya, T., Kamita, M., Tsuchida, A., Wilber, H., Yamada, T., Honda, K.	*ACTN4* copy number as a predictive biomarker for chemoradio-therapy of locally advanced pancreatic cancer.	Br. J. Cancer	112	704-13	2015

Masuda, M., Yamada, T.	Signaling pathway profiling by reverse-phase protein array for personalized cancer medicine.	Biochim Biophys Acta.	1854	651-657	2015
Tanaka, N., Yamashita, T., Yamamoto, S., Matsunobu, T., Tsuda, H., Honda, K., Yamada, T., Tamai, S., Shiotani, A.	Histological growth pattern of and alpha-actinin-4 expression in thyroid cancer.	Anticancer Res.	34	3157-63	2014
Watabe, Y., Mori, T., Yoshimoto, S., Nomura, T., Shibahara, T., Yamada, T., Honda, K.	Copy number increase of ACTN4 is a prognostic indicator in salivary gland carcinoma.	Cancer Med.	3	613-22	2014
Masuda, M., Chen, WY., Miyanaga, A., Nakamura, Y., Kawasaki, K., Sakuma, T., Ono, M., Chen, CL., Honda, K., Yamada, T.	Alternative mammalian target of rapamycin (mTOR) signal activation in sorafenib-resistant hepatocellular carcinoma cells revealed by array-based pathway profiling.	Mol. Cell. Proteomics	13	1429-38	2014
Yamada, T.	Reverse phase protein array: a tool for signaling pathway profiling in the era of genome resequencing.	Dig. Dis. Sci.	59	895-6	2014
Matsukawa, S., Morita, K., Negishi, A., Harada, H., Nakajima, Y., Shimamoto, H., Tomioka, H., Tanaka, K., Ono, M., Yamada, T., Omura, K.	Galectin-7 as a potential predictive marker of chemo- and/or radio- therapy resistance in oral squamous cell carcinoma.	Cancer Med.	3	349-61	2014

Yumimoto, K., Akiyoshi, S., Ueo, H., Sagara, Y., Onoyama, I., Ueo, H., Ohno, S., Mori, M., Mimori, K., Nakayama, K.I.	F-box protein Fbxw7 inhibits cancer metastasis in a non-cell-autonomous manner.	J. Clin. Invest.	125	621-35	2015
Adachi, S., Homoto, M., Tanaka, R., Hioki, Y., Murakami, H., Suga, H., Matsumoto, M., Nakayama, K.I., Hatta, T., Iemura, S., Natsume, T.	ZFP36L1 and ZFP36L2 control LDLR mRNA stability via the ERK-RSK pathway.	Nucleic Acids Res.	42	10037-49	2014
Saita, S., Shirane, M., Ishitani, T., Shimizu, N., Nakayama, K.I.	Role of the ANKMY2-FKBP38 axis in regulation of the Sonic hedgehog (Shh) signaling Pathway.	J. Biol. Chem.	289	25639-54	2014
Yamauchi, T., Nishiyama, M., Moroishi, T., Yumimoto, K., Nakayama, K.I.	MDM2 mediates nonproteolytic polyubiquity-lation of the DEAD-Box RNA helicase DDX24.	Mol. Cell. Biol.	34	3321-40	2014
Yugi, K., Kubota, H., Toyoshima, Y., Noguchi, R., Kawata, K., Komori, Y., Uda, S., Kunida, K., Tomizawa, Y., Funato, Y., Miki, H., Matsumoto, M., Nakayama, K.I., Kashikura, K., Endo, K., Ikeda, K., Soga, T., Kuroda, S.	Reconstruction of insulin signal flow from phospho-proteome and metabolome data.	Cell Rep.	8	1171-83	2014

Kitagawa, K., Shibata, K., Matsumoto, A., Matsumoto, M., Ohhata, T., Nakayama, K.I., Niida, H., Kitagawa, M.	Fbw7 targets GATA3 through cyclin-dependent kinase 2-dependent proteolysis and contributes to regulation of T-cell development.	Mol. Cell. Biol.	34	2732-44	2014
Kanatsu-Shinohara, M., Onoyama, I., Nakayama, K.I., Shinohara, T.	Skp1-Cullin-F-box (SCF)-type ubiquitin ligase FBXW7 negatively regulates spermatogonial stem cell self-renewal.	Proc. Natl. Acad. Sci. USA	111	8826-31	2014
Moroishi, T., Yamauchi, T., Nishiyama, M., Nakayama, K.I.	HERC2 targets the iron regulator FBXL5 for degradation and modulates iron metabolism.	J. Biol. Chem.	289	16430-41	2014
Matsumoto, A., Takeishi, S., Nakayama, K.I.	p57 regulates T-cell development and prevents lymphomagenesis by balancing p53 activity and pre-TCR signaling.	Blood	123	3429-39	2014
Hashiguchi, T., Oyamada, A., Sakuraba, K., Shimoda, K., Nakayama, K.I., Iwamoto, Y., Yoshikai, Y., Yamada, H.	Tyk2-dependent bystander activation of conventional and nonconventional Th1 cell subsets contributes to innate host defense against Listeria monocytogenes infection.	J. Immunol.	192	4739-47	2014
Hashimoto, Y., Shirane, M., Matsuzaki, F., Saita, S., Ohnishi, T., Nakayama, K.I.	Protrudin regulates endoplasmic reticulum morphology and function associated with the pathogenesis of hereditary spastic paraplegia.	J. Biol. Chem.	289	12946-61	2014

Journal of proteome research

Article

pubs.acs.org/jpr

Proteome-Wide Discovery of Unknown ATP-Binding Proteins and Kinase Inhibitor Target Proteins Using an ATP Probe

Jun Adachi,* Marina Kishida, Shio Watanabe, Yuuki Hashimoto, Kazuna Fukamizu, and Takeshi Tomonaga*

Laboratory of Proteome Research, National Institute of Biomedical Innovation, Ibaraki, Osaka 567-0085, Japan

Supporting Information

ABSTRACT: ATP-binding proteins, including protein kinases, play essential roles in many biological and pathological processes and thus these proteins are attractive as drug targets. Acyl-ATP probes have been developed as efficient probes for kinase enrichment, and these probes have also been used to enrich other ATP-binding proteins. However, a robust method to identify ATP-binding proteins with systematic elimination of nonspecific binding proteins has yet to be established. Here, we describe an ATP competition assay that permitted establishment of a rigorous ATP-binding protein list with virtual elimination of nonspecific proteins. A total of 539 ATP-binding protein candidates were identified, including 178 novel candidates. In informatics analysis, ribosomal proteins were overrepresented in the list of novel candidates. We also found multiple ATP-competitive sites for several kinases, including epidermal growth factor receptor, serine/threonine-protein kinase PRP4 homologue, cyclin-dependent kinase 12, eukaryotic elongation factor 2 kinase, ribosomal protein S6 kinase alpha-1, and SRSF protein kinase 1. Using our cataloged ATP-binding protein list, a selectivity profiling method that covers the kinome and ATPome was established to identify off-target binding sites of ATP-competitive kinase inhibitors, staurosporine and crizotinib.

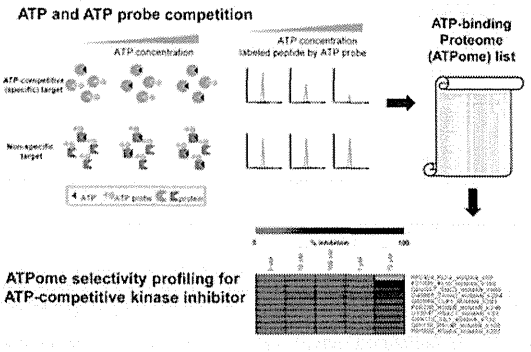

KEYWORDS: *Chemical proteomics, ATP-binding proteins, ATP-competitive kinase inhibitor*

INTRODUCTION

Adenosine triphosphate (ATP) is an abundant nucleoside triphosphate that is often referred to as the "molecular unit of currency" of intracellular energy transfer.[1] ATP binds to numerous proteins that play pivotal roles in most cellular processes, including metabolism, synthesis, active transport, cell signaling, and maintenance of cell structure. The phosphate-binding loop (P-loop) is a particular motif found in ATP- and guanosine triphosphate (GTP)-binding proteins.[2] The P-loop was originally identified as a conserved motif in the α- and β-subunits of ATP synthases, myosin, and kinases;[2a] however, this motif is not found in all ATP-binding proteins.

There are almost 1500 proteins that are assigned as ATP-binding proteins in the UniProt database; however, the whole picture of the ATP-binding proteome (ATPome) is still unclear. Affinity chromatography using ATP-immobilized sepharose beads[3] or kinase inhibitor-immobilized beads [4] have often been used to identify ATP-binding proteins. Recently, biotin-conjugated acyl-ATP probes have also been developed for large-scale identification of ATP-binding proteins.[5] Using biotin-conjugated acyl-ATP probes, lysine residues of target proteins can be covalently labeled by the probe, thus allowing enrichment of labeled proteins or peptides using streptavidin beads. This superior probe design allows reduced sample complexity and increases the sensitivity. Furthermore, ATP-binding sites or regions can be identified from mass spectrometry-based identification of labeled peptides. This information is particularly valuable because ATP-binding sites are key residues modulating enzyme activity.[6]

This kind of probe has been used for kinome analysis[7] and analysis of other ATP-binding proteins.[7a,8] In mammalian cells, 551 proteins were identified in HeLa-S3 cells using a desthiobiotin-conjugated ATP-affinity probe.[8a] Also, 122 ATP-binding proteins in *Mycobacterium tuberculosis* and 242 labeled sites in *Arabidopsis thaliana* were identified using similar probes.[8b,c] These large-scale studies suggest that enrichment based on biotin-streptavidin affinity will enable sensitive and large-scale identification of the ATPome.

Despite this progress, the acyl-ATP probe has the disadvantage of reacting nonspecifically with lysine residues that are not in ATP-binding sites. It was reported that only 11% of all identified peptides were considered to belong to the possible ATP-binding proteins.[8a] These data suggest that nonspecific labeling is more dominant than specific labeling. In kinome analysis, this disadvantage of an acyl-ATP probe is not a major problem because conserved lysine targets near the ATP-binding site are known;[7b] thus, it is possible to distinguish nonspecific from

Received: April 9, 2014
Published: September 17, 2014

specific labeled peptides using the amino acid sequences of identified peptides. However, for other ATP-binding proteins, it is difficult to predict ATP-binding sites or regions because the P-loop motif is not conserved in all proteins. For this reason, a systematic and robust method is required that allows identification and quantification of ATP-binding proteins and residues on a global proteome scale with minimum contamination by nonspecific binding proteins. Moreover, development of novel methodology for ATPome analysis will contribute to decoding of ATP−protein interactions and understanding of the regulatory mechanisms of ATP-dependent protein functions, both of which are crucial in the design of ATP-competitive inhibitors for drug discovery.

An acyl-ATP probe has also been used for identification of off-target proteins of ATP-competitive kinase inhibitors, using competitive binding studies.[5b,7b] Although various methods have been developed for selectivity profiling of kinase inhibitors, including the acyl-ATP probe, most of these methods are limited to kinase targets.[7b,9] However, kinase inhibitors can also inhibit other proteins.[4b,10] Thus, a selectivity profiling method for ATP-competitive inhibitors that covers kinases and other ATP-binding proteins will give more off-target information and contribute to understanding the molecular mechanism of action of kinase inhibitors.

In this study, we developed a straightforward and robust strategy using ATP and ATP probe competition to distinguish ATP-binding proteins from nonspecific labeled proteins using quantitative proteomic analysis. Our ATPome analysis enabled systematic elimination of nonspecific labeled proteins and establishment of a rigorous ATPome list. Using this list, we proved our concept of expanding targets from the kinome to the ATPome for selectivity profiling of ATP-competitive kinase inhibitors.

EXPERIMENTAL DETAILS

Materials

An ActivX desthiobiotin-ATP probe, Halt protease/phosphatase inhibitor cocktail, Zeba spin desalting column (7K MWCO), and high-capacity-binding streptavidin agarose were obtained from Thermo Scientific (Rockford, IL). Modified trypsin, complete protease inhibitor cocktail, and PhosSTOP phosphatase inhibitor cocktail were purchased from Roche Applied Science (Mannheim, Germany). Dulbecco's modified Eagle's medium (DMEM), fetal bovine serum (FBS), dialyzed FBS, penicillin, and streptomycin were from Life Technologies (Carlsbad, CA). (*S*)-Crizotinib was obtained from APEXbio (Houston, TX). $^{13}C_6$,$^{15}N_4$-L-arginine hydrochloride and $^{13}C_6$,$^{15}N_2$-L-lysine hydrochloride were purchased from Cambridge Isotope Laboratories (Tewksbury, MA). Unless otherwise noted, all other chemicals were obtained from Wako (Osaka, Japan).

Cell Culture and Lysis

HeLa-S3 cells for label-free experiments were grown in DMEM with 10% fetal bovine serum plus antibiotics in 10% CO_2 at 37 °C. HeLa-S3 cells for SILAC experiments were cultured in DMEM as described by Ong et al.[11] Briefly, DMEM was supplemented with 10% dialyzed fetal bovine serum and either 28.0 mg/L normal isotopic abundance arginine and 48.7 mg/L normal isotopic abundance lysine (light) or 28.0 mg/L arginine with six ^{13}C and four ^{15}N atoms and 48.7 mg/L lysine with six ^{13}C and two ^{15}N atoms (heavy). The efficiency of labeling was estimated to be 99.5% for lysine and 98.5% for arginine after five passages, and labeled cells were used for spike-in SILAC experiments. Approximately 5×10^8 cells were centrifuged, washed with cold phosphate-buffered saline (PBS), and lysed with 5 mL of ice-cold lysis buffer (25 mM Tris, pH 7.5, 150 mM NaCl, 1% CHAPS, 1% Nonidet P-40, protease inhibitor cocktail, and phosphatase inhibitor cocktail). The lysate was aliquoted, snap-frozen in liquid nitrogen, and stored at −80 °C.

ATP Probe Labeling, In-Solution Digestion, and Affinity Purification

Cell lysate was centrifuged at 16 000*g* at 4 °C for 5 min, and the resulting supernatant was collected and subjected to gel filtration using a Zeba spin column (Pierce) to remove free endogenous ATP, ADP, and small molecules. Halt protease/phosphatase inhibitor cocktail was then added to the sample. Protein concentrations were determined by DC protein assay (Bio-Rad, Hercules, CA), and the cell lysate was diluted with reaction buffer (20 mM Hepes, pH 7.5, 150 mM NaCl, 0.1% Triton X-100) to a final protein concentration of 4 mg/mL. $MnCl_2$ was added to 250 μL of lysate (1 mg of protein) at a final concentration of 20 mM. The labeling reaction in the ATP-competition assay was carried out at a final concentration of 5 μM ATP probe at room temperature with gentle shaking for 10 min, following preincubation with ATP for 10 min. After the reaction, the sample was denatured by 5 M urea, reduced with DTT (5 mM final concentration), and alkylated with iodoacetamide (20 mM final concentration). The labeling reaction in the kinase inhibitor experiment was performed similarly, with minor modifications. Kinase inhibitors were preincubated for 10 min with SILAC-labeled light lysate (1 mg of protein), whereas SILAC-labeled heavy lysate (1 mg of protein) was not treated with kinase inhibitors. Concentrations of kinase inhibitors were determined to cover IC_{50} values from previous studies.[7b] After denaturation with urea, heavy lysate was spiked into an equal amount of light lysate. After the alkylation step, the solution was substituted by digestion buffer by gel filtration followed by digestion at 37 °C overnight with sequencing-grade trypsin at an enzyme/substrate ratio of 1:100. Immobilized streptavidin agarose resin was used to capture the labeled peptides. Prior to binding, 50 μL of slurry was washed three times with 500 μL of elution buffer (50% acetonitrile, 0.1% TFA) and three times with 500 μL of digestion buffer. After addition to the digested peptide solution, the mixture was incubated at room temperature for 1 h with gentle rotation. To remove the unbound peptides, agarose resin was extensively washed with 2 mL of washing buffer (25 mM Tris-HCl, pH 7.4, 150 mM NaCl, 1 mM EDTA, 1% Nonidet P-40, and 5% glycerol), 2 mL of PBS, and 2 mL of pure H_2O. After washing, labeled peptides were eluted with 150 μL of elution buffer (50% ACN, 0.1% TFA) twice and dried in a SpeedVac. Peptides were dissolved in 50 μL of 2 M urea and 1% TFA and desalted using StageTips.[12] Each experiment was performed in triplicate or quadruplicate.

LC−MS/MS Analysis

StageTip-purified peptides were eluted in a final volume of 10 μL. Liquid chromatography was performed with an UltiMate 3000 Nano LC system (Thermo Scientific) and a HTC-PAL autosampler (CTC Analytics, Zwingen, Switzerland). Peptides were separated on a fused silica column (300 mm length × 75 μm i.d.) packed in-house with reverse-phase material ReproSil-Pur C18-AQ, 1.9 μm resin (Dr. Maisch, Ammerbuch-Entringen, Germany) at 60 °C. The mobile phases consisted of buffer A (0.1% formic acid and 2% acetonitrile) and B (0.1% formic acid and 90% acetonitrile). Samples were dissolved in 1% TFA and 2% acetonitrile and loaded onto a trap column (0.075 × 20 mm,

Acclaim PepMap RSLC Nano-Trap Column; Thermo Scientific). The nanoLC gradient was delivered at 280 nL/min and consisted of a linear gradient of buffer B developed from 5 to 30% B in 85 min. The Q Exactive instrument was operated in data-dependent mode. Survey full-scan MS spectra (m/z 350−1800) were acquired in the Orbitrap with a resolution of 70 000 after accumulation of ions to a 3×10^6 target value. Dynamic exclusion was set to 20 s. The 12 most intense multiply charged ions ($z \geq 2$) were sequentially accumulated to a 2×10^5 target value and fragmented in the octopole collision cell by higher-energy collisional dissociation (HCD) with a maximum injection time of 120 ms and a resolution of 35 000. Typical mass spectrometric conditions were as follows: spray voltage, 2 kV; no sheath and auxiliary gas flow; heated capillary temperature, 250 °C; normalized HCD collision energy, 25%. The MS/MS ion selection threshold was set to 5×10^4 counts. A 3.0 Da isolation width was chosen.

Analysis of Proteomic Data

Raw data were processed by MaxQuant 1.3.0.5 supported by the Andromeda search engine for peptide identification.[13] MaxQuant was used to score peptides for identification based on a search with an initial allowed mass deviation of the precursor ion of up to 7 ppm. The allowed fragment mass deviation was 20 ppm. Search of MS/MS spectra against the UniProt human database (release 2011_11) combined with 262 common contaminants was performed using the Andromeda search engine. Enzyme specificity was set as C-terminal to Arg and Lys with allowed cleavage at proline bonds and a maximum of three missed cleavages. Carbamidomethylation of cysteine was set as a fixed modification, and methionine oxidation and desthiobiotinylated lysine (+196.1212 Da), as variable modifications. Peptides and proteins were accepted with a false discovery rate of <1%, which was estimated on the basis of the number of accepted hits from the reverse database. Feature matching between raw files was enabled for ATP competition data sets using a retention time window of 2 min. To extract ATP-competitive peptides/sites from label-free quantitation data, we removed peptides that were inhibited by <80% at 10 μM ATP. Peptides with quantitation values that were not reproducible were also rejected, based on an average of <0.5 for three correlation coefficients of intensity values in triplicate experiments (correlation coefficients of experiments 1 and 2, 2 and 3, 3 and 1); 89.6% of peptides were rejected by this filter. MS spectra for all ATP-competitive peptides were checked for missed assignments by matching between raw files, and 946 peptides (4.3% of all peptides) passed all criteria and were recognized as ATP-competitive peptides. In the kinase inhibitor experiment, spike-in SILAC quantitation was used instead of label-free quantitation. Peptides inhibited by >50% at 10 μM staurosporine were accepted. MS spectra for all target peptides were checked manually. A list of identified proteins and peptides is given in Supporting Information Table S1.

RESULTS AND DISCUSSION

Rigorous ATP-Binding Proteome (ATPome) Analysis

Chemical proteomic analysis is an important approach for large-scale ATPome analysis.[7a,8] However, nonspecific chemical labeling is unavoidable because the acyl phosphate group of the probe can react with lysine residues that are not located near the ATP-binding site in addition to conserved lysine residues in the ATP-binding site. In previous reports,[8b,c] all proteins labeled by an ATP probe were recognized as ATP-binding proteins. This is because experiments were not designed to distinguish specific proteins from nonspecific proteins. In a report considering nonspecific binding of an acyl ATP probe, low (10 μM) and high (100 μM) concentrations of the probe were used in the labeling step to distinguish specific from nonspecific labeling.[8a] This strategy is based on the hypothesis that specific labeling reactions are more likely to occur at low concentration, relative to nonspecific labeling, and this strategy was shown to be applicable for some ATP-binding proteins.[8a] However, it may be difficult to identify the entire ATPome using this strategy because apparent dissociation constants of ATP with kinases were reported to vary by more than 3 orders of magnitude.[7b]

To address this problem, we used a simple strategy of ATP and ATP probe competition to distinguish specific and nonspecific labeling (Figure 1). Six concentrations of ATP (final

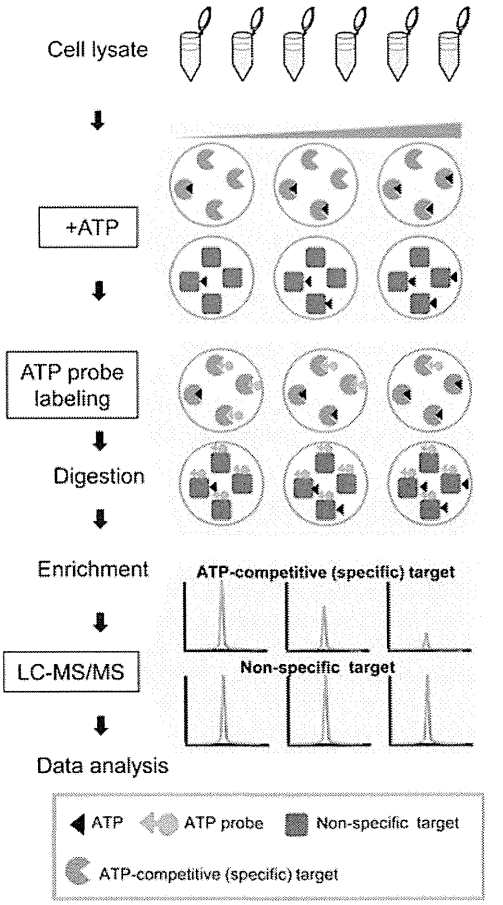

Figure 1. Schematic of the ATP and ATP probe competition assay to identify ATP-binding proteins.

concentrations: 0 nM, 100 nM, 1 μM, 10 μM, 100 μM, and 1 mM) were added to cell lysates following a desalting step to remove endogenous ATP. Then, the ATP probe was added to each cell lysate to label lysine residues under competition with ATP. Lysine residues were categorized on the basis of dose-dependent inhibition profiles showing specific and nonspecific labeling.

Mass spectrometry (MS) properties also affect peptide sequence detection, and it has been shown that high-resolution MS and MS/MS are suitable for modified peptide identification.[14] In previous studies, low–low (low-resolution MS and

Table 1. Identified, Quantified, and ATP-Competitive Peptides in Each Kinase Family

	identified				quantified			ATP competitive		
	total	VAIK	HRD	others	VAIK	HRD	others	VAIK	HRD	others
AGC	156	23	27	106	20	19	52	16	13	26
atypical	179	6	1	172	3	0	98	2	0	15
CAMK	80	20	21	39	17	17	19	11	11	7
CK1	22	0	8	14	0	8	11	0	6	5
MGC	140	20	38	82	17	33	42	11	21	21
other	103	15	30	58	10	27	30	6	19	9
STE	169	20	23	116	25	19	51	12	6	23
TK	84	22	0	82	17	0	36	12	0	25
TKL	32	7	9	16	6	5	6	5	3	1
total	965	143	157	665	115	128	345	75	79	132

MS/MS) and high–low (high-resolution MS and low-resolution MS/MS) strategies have been used for identification of ATP probe-labeled peptides.[7a,b,d,8a] In this study, we used a high–high strategy (high-resolution MS and MS/MS)[15] for accurate site identification of target lysine residues to create a rigorous ATPome list. A total of 22 236 labeled peptides were identified with FDR <1%, and 794 peptides showed ATP-competitive profiles in triplicate experiments. At the protein level, 539 protein groups were identified as ATP-binding protein candidates, including 178 candidates that are not assigned as ATP-binding protein in the UniProt database. On the basis of large-scale proteome data for HeLa cells,[16] 7781 proteins were identified in total, and 868 were ATP-binding proteins. Thus, of the 1479 assigned ATP-binding proteins in the UniProt database, 58.7% (868/1479) were identified in HeLa cells. Nonidentified proteins might have low abundancy, may not be expressed in the cells, or may have amino acid sequences that are not suitable for MS detection. Therefore, the 868 identified ATP-binding proteins are considered to be MS-detectable ATP-binding proteins in HeLa cells using state-of-the-art MS technology.

Of the 539 ATP-binding protein candidates identified in our study, 495 were included in the large-scale HeLa proteome data. Thus, if we assume that 868 ATP-binding proteins in the database are MS-detectable ATP-binding proteins in HeLa and HeLa-S3 cells, then the sensitivity of our ATP competition assay is 57.0% (495/868). This value is only a rough estimate because it does not include differences between the previous and current studies, including modification of peptides (unmodified vs labeled peptides), cell lines (HeLa vs HeLa-S3), and instruments. Sensitivity can be calculated more precisely with greater accumulation of ATPome data. It is also difficult to discuss the specificity of our identified ATP-binding protein candidates because of the lack of a large-scale validation method. However, 361 of these proteins (67.0%) were assigned as ATP-binding proteins in the UniProt database. We anticipate that the other 178 proteins will eventually be confirmed as ATP-binding proteins by the scientific community.

Kinases Identified in ATPome Analysis

All protein kinases have at least one of two reactive lysine residues in the ATP-binding pocket: one is found in the ATP binding loop region in the VAIK motif in all protein kinases except WNK, whereas the other is located two residues to the C-terminal side of the catalytic aspartic acid in the HRD motif in most serine/threonine kinases.[5b] From our data set, 220 kinase groups were identified. As shown in Table 1, a total of 965 peptides were identified, of which 143 and 157 contained a lysine residue in the VAIK motif and close to the HRD motif, respectively, and 665 (68.9% of all the identified peptides) had a lysine from another kinase region. Thus, these data show that most identified peptides were not from the expected regions of kinases; however, the intensity level of peptides containing the VAIK or HRD motif was 4.9-fold higher than that of other peptides on a 50% height cumulative plot (Figure 2). Thus, these data suggest that the reactivity of the ATP probe with the two conserved lysine residues is higher than that with other lysine residues.

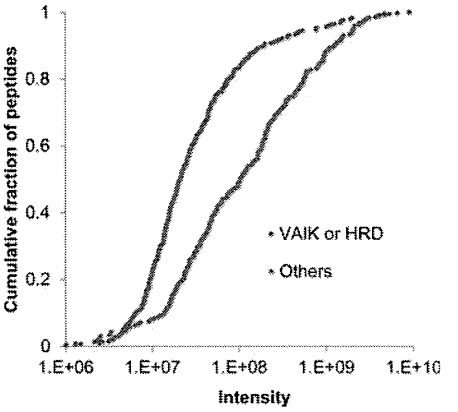

Figure 2. Comparison of peak intensity distributions between peptides containing conserved lysine residues near the VAIK or HRD motif and other peptides.

ATP-competitive profiles were found for the expected peptides containing lysine residues in the ATP-binding pocket as well as for peptides containing other lysine residues. For example, nine lysine residues were identified from the kinase domain of EGFR, and five were quantified (Figure 3). All of the quantified peptides showed similar dose-dependent competition profiles. Among these lysines, K745 (IPVAIK(de)ELR) in the VAIK motif binds to ATP, and K860 and K875 have also been reported to be ATP-binding sites.[8a] These residues are close to D855, which is part of the DFG motif assigned as an ATP-binding site in the UniProt database. The two other sites, K716 and K867, have not previously been recognized as ATP-binding sites. Multiple ATP-binding sites were also identified on other proteins, including eight sites on serine/threonine-protein kinase PRP4 homologue, and four on cyclin-dependent kinase 12, eukaryotic elongation factor 2 kinase, ribosomal protein S6 kinase alpha-1, and SRSF protein kinase 1. These data suggest that multiple residues located in ATP-binding pockets and other regions are involved in ATP-kinase interactions. It will be

dx.doi.org/10.1021/pr500845u | J. Proteome Res. 2014, 13, 5461–5470

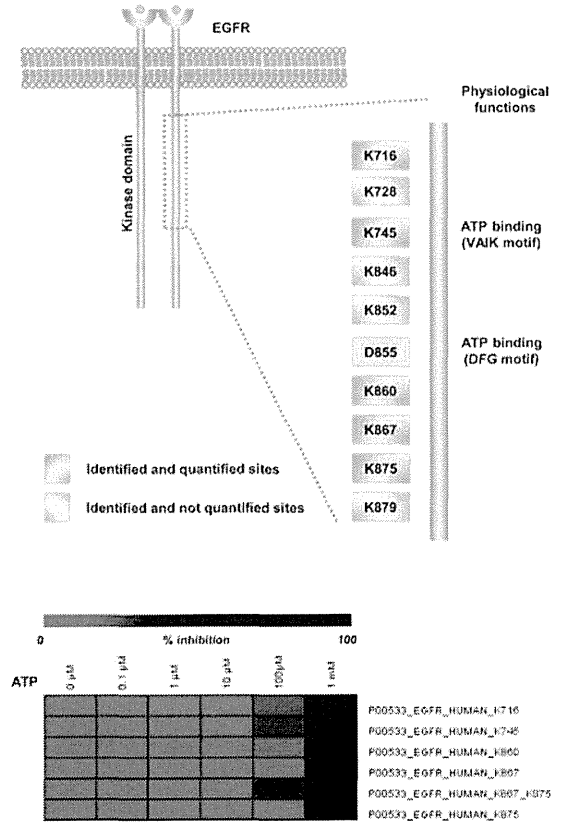

Figure 3. ATP-competitive sites of EGF receptor and their competition profiles.

important to determine the biological functions of these interactions, and our site-specific data will permit the generation of mutated proteins for site-specific functional analysis.

Other Proteins Identified in ATPome Analysis

In addition to kinases, 360 protein families/groups were identified as ATP-binding protein candidates using the ATP competition assay (Table 2). These included 130 protein families/groups that were classified into 17 major ATP-binding protein families. Most were assigned as ATP-binding proteins in the UniProt database. For example, 50 lysine residues (10 protein groups) were identified from the ATP-binding cassette (ABC) transporter family (Figure 4). Twelve of these lysine residues were located in ATP-binding regions based on a database search, 11 showed dose-dependent competition profiles, and 8 met our stringent criteria to be kept as candidate sites for ATP binding. The three other sites in the ATP-binding region did not meet our criteria due to quantitative variability between experiments (see Experimental Details). This finding suggests that true negative results are present in the data. However, we used stringent criteria because we placed a priority on the confidence of our ATPome list. Four lysine residues (ABCB6_K836, MRP4_K633, ABCE1_K169, and ABCE1_K250) with ATP-competitive profiles were also identified despite these sites not being located in a conserved ATP-binding region. The biological importance of these lysines is unknown, but the rigor of our data should provide confidence in future biological functions identified for these residues.

Table 2. ATP-Binding Proteins Identified Using an ATP Competition Approach in This Study

protein family/group	ATP binding proteins confirmed by ATP competition	UniProt assigned[a]	UniProt not assigned[b]
protein kinase	179	179	0
small molecule kinases/ phosphotransferases	31	31	0
AAA ATPase family	15	15	0
aminoacyl-tRNA synthetases	10	10	0
ATP GRASP domain proteins	10	10	0
HSP90 family	8	8	0
HSP70 family	8	8	0
ABC Transporters	8	8	0
DEAD box helicase family	8	8	0
other AAA+ members	7	5	2
ubiquitin-activating E1 enzymes	5	5	0
chaperonins and related proteins	4	4	0
actins	4	4	0
MCM family	3	3	0
nudix hydrolases	3	0	3
HSP110 family	2	2	0
HSP40 family	2	0	2
dynein heavy chain family	2	2	0
others	230	59	171
total	539	361	178

[a]Proteins assigned as ATP-binding protein. [b]Proteins not assigned as ATP-binding protein.

Bioinformatics Analysis of the ATPome

Our ATPome list contains 230 ATP-binding protein candidates that do not belong to the major 17 ATP-binding protein families/groups (Table 2). Of these, 59 proteins were already assigned as ATP-binding proteins in the UniProt database, but 171 proteins were not assigned. Gene ontology (GO) analysis revealed that GO terms related to ribosome were significantly overrepresented in these 171 proteins ($p < 0.0001$, Table 4), whereas GO terms related to ATP-binding and kinases were strongly overrepresented in all ATP-binding protein candidates, as expected (Table 3). Protein synthesis is one of the most ATP-consuming processes in mammalian cells;[17] thus, the high number of ribosome-related terms is reasonable. Among the ribosomal proteins that showed dose-dependent competition profiles (Supporting Information Figure 2), RPS9, RPL7a, and RPS6 have previously been identified as ATP-binding proteins.[7a] Another 11 of the ribosomal proteins have not been previously reported to be ATP-binding proteins.

We also tried to find ATP-binding motifs using our rigorous and large-scale data set. In an initial analysis of motifs for identified kinases, the expected conserved HRD motif (HxDxKxxN) located in subdomain VIB and the VAIK motif (VAxK and GxxxAxK) in subdomain II were identified using a motif-X software tool[18] (Figure 5A). Analysis of AAA+ ATPases also resulted in identification of the well-known P-loop sequence motif (Figure 5B). We also looked for sequence motifs for ATP-binding protein candidates that were not assigned in the UniProt database; however, no significant motif was identified. Thus, structural analysis at the molecular level is needed to understand

dx.doi.org/10.1021/pr500845u | J. Proteome Res. 2014, 13, 5461−5470

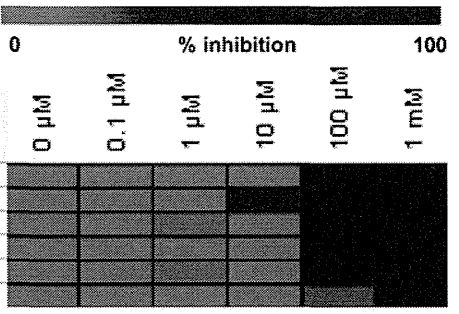

Gene Names	Site	ATP binding region	ATP competitive?
ABCB6	629	623 – 630	yes
ABCB6	836	623 – 630	yes
ABCB8	513	507 – 514	yes
ABCC4	633	445 – 452, 1075 – 1082	yes
ABCC4	1081	445 – 452, 1075 – 1082	yes
ABCC5	1233	595 – 602, 1227 – 1234	
ABCC11	1181	544 – 551, 1175 – 1182	
ABCC12	1160	513 – 520, 1154 – 1161	
ABCD3	38	473 – 480	
ABCD3	399	473 – 480	
ABCD3	39	473 – 480	
ABCD4	427	421 – 428	yes
ABCE1	250	110 – 117, 379 – 386	yes
ABCE1	169	110 – 117, 379 – 386	yes
ABCE1	116	110 – 117, 379 – 386	yes
ABCE1	181	110 – 117, 379 – 386	
ABCE1	126	110 – 117, 379 – 386	
ABCE1	165	110 – 117, 379 – 386	
ABCE1	419	110 – 117, 379 – 386	
ABCE1	64	110 – 117, 379 – 386	
ABCE1	584	110 – 117, 379 – 386	
ABCE1	431	110 – 117, 379 – 386	
ABCE1	121	110 – 117, 379 – 386	
ABCF1	256	336 – 343, 658 – 665	
ABCF1	192	336 – 343, 658 – 665	
ABCF1	174	336 – 343, 658 – 665	
ABCF1	342	336 – 343, 658 – 665	
ABCF1	85	336 – 343, 658 – 665	
ABCF1	39	336 – 343, 658 – 665	
ABCF1	414	336 – 343, 658 – 665	
ABCF1	389	336 – 343, 658 – 665	
ABCF1	340	336 – 343, 658 – 665	
ABCF1	211	336 – 343, 658 – 665	
ABCF2	436	118 – 125, 430 – 437	yes
ABCF2	66	118 – 125, 430 – 437	
ABCF2	351	118 – 125, 430 – 437	
ABCF2	461	118 – 125, 430 – 437	
ABCF2	404	118 – 125, 430 – 437	
ABCF2	25	118 – 125, 430 – 437	
ABCF2	456	118 – 125, 430 – 437	
ABCF2	326	118 – 125, 430 – 437	
ABCF2	304	118 – 125, 430 – 437	
ABCF2	618	118 – 125, 430 – 437	
ABCF2	522	118 – 125, 430 – 437	
ABCF2	359	118 – 125, 430 – 437	
ABCF2	608	118 – 125, 430 – 437	
ABCF2	602	118 – 125, 430 – 437	
ABCF2	508	118 – 125, 430 – 437	
ABCF3	531	210 – 217, 525 – 532	yes
ABCF3	216	210 – 217, 525 – 532	yes
ABCF3	457	210 – 217, 525 – 532	
ABCF3	531	210 – 217, 525 – 532	

Figure 4. ATP competitive sites and competition profiles of ATP-binding cassette (ABC) transporter family.

the interactions between ATP and the ATP-binding protein candidates identified in this study.

Selectivity Profiling of Kinase Inhibitors Using an Acyl-ATP Probe

The sensitivity and throughput of target selectivity profiling of kinase inhibitors using an acyl-ATP probe have improved,[19,7d] but only kinases have previously been selected as profiling targets. However, it is possible that ATP-competitive kinase inhibitors inhibit other ATP-binding proteins. Therefore, we expanded our targets and performed ATPome profiling in HeLa-S3 cell lysate. Staurosporine was used as a test inhibitor because of its established wide specificity for multiple target kinases.

Selectivity profiling of ATPome was performed using the spike-in SILAC method.[20] As shown in Figure 6, 69 peptides identified from kinases and 10 peptides identified from other ATP binding proteins showed dose-dependent inhibition

Table 3. Significantly Overrepresented GO Terms for Identified ATP-Binding Proteins

GO term	*P* value	fold enrichment	Benjamini–Hochberg
GO:0005524~ATP binding	4.83×10^{-146}	4.42	1.57×10^{-143}
GO:0032559~adenyl ribonucleotide binding	3.45×10^{-146}	4.40	2.24×10^{-143}
GO:0030554~adenyl nucleotide binding	1.27×10^{-143}	4.25	2.74×10^{-141}
GO:0001882~nucleoside binding	4.11×10^{-143}	4.19	6.66×10^{-141}
GO:0001883~purine nucleoside binding	7.69×10^{-142}	4.20	9.98×10^{-140}
GO:0032555~purine ribonucleotide binding	2.92×10^{-124}	3.68	3.16×10^{-122}
GO:0032553~ribonucleotide binding	2.92×10^{-124}	3.68	3.16×10^{-122}
GO:0017076~purine nucleotide binding	2.17×10^{-122}	3.58	2.01×10^{-120}
GO:0000166~nucleotide binding	1.43×10^{-108}	3.09	1.16×10^{-106}
GO:0006468~protein amino acid phosphorylation	7.14×10^{-72}	5.89	1.54×10^{-68}
GO:0004672~protein kinase activity	2.54×10^{-69}	5.60	1.83×10^{-67}
GO:0004674~protein serine/threonine kinase activity	3.02×10^{-64}	6.24	1.96×10^{-62}
GO:0016310~phosphorylation	1.64×10^{-64}	4.80	1.76×10^{-61}
GO:0006796~phosphate metabolic process	1.12×10^{-52}	3.96	8.00×10^{-50}
GO:0006793~phosphorus metabolic process	1.12×10^{-52}	3.96	8.00×10^{-50}

Table 4. Significantly Overrepresented GO Terms for Identified but Nonassigned ATP-Binding Proteins

GO term	*P* value	fold enrichment	Benjamini–Hochberg
GO:0006414~translational elongation	1.23×10^{-11}	8.61	1.05×10^{-8}
GO:0022626~cytosolic ribosome	2.47×10^{-8}	7.49	5.73×10^{-6}
GO:0022625~cytosolic large ribosomal subunit	1.12×10^{-6}	10.72	6.51×10^{-5}
GO:0030529~ribonucleo protein complex	6.08×10^{-7}	2.80	7.05×10^{-5}
GO:0044445~cytosolic part	1.06×10^{-6}	5.04	8.19×10^{-5}
GO:0033279~ribosomal subunit	4.63×10^{-6}	4.83	2.15×10^{-4}
GO:0003735~structural constituent of ribosome	2.38×10^{-6}	4.73	7.44×10^{-4}
GO:0005840~ribosome	2.22×10^{-5}	3.67	8.59×10^{-4}

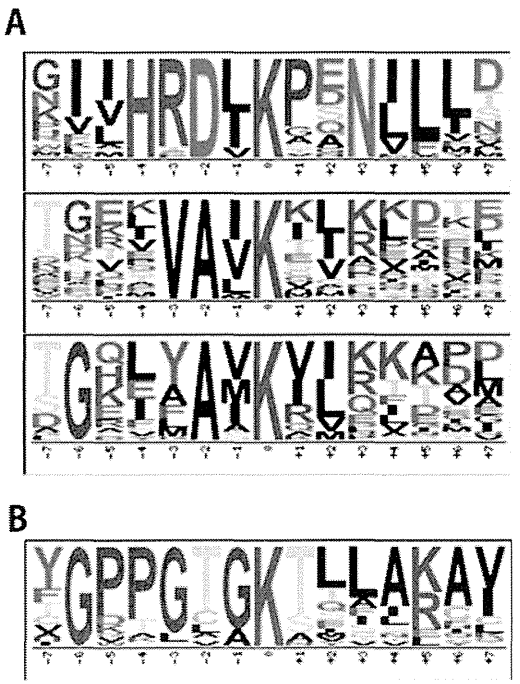

Figure 5. Motif analysis of ATP competitive sites on kinases and AAA+ ATPases.

profiles. Similar kinome profiling results were found to those obtained in previous studies using an acyl-ATP probe[7b] or competition binding assays using recombinant kinases.[21] However, protein kinase C (PKC), a well-known target of staurosporine, was not identified using our method. We found that a peptide containing the VAIK motif of protein kinase C-alpha (ETGNHYAMK(de)ILDK) was identified in two LC–MS/MS runs, but this peptide was not quantified in both cases. Weak intensity seems to be the major reason that this peptide was identified only in two runs and without quantification. Therefore, there is a need to increase the sensitivity using targeted analysis[7b] to detect targets with weak intensity. We also found 10 other ATP-binding proteins (10 lysine residues) with dose-dependent inhibition profiles. These 10 lysines were confirmed to be ATP-competitive in our ATP competition assay. Therefore, it is possible that these lysines are not nonspecific targets but are specific targets of staurosporine. The 10 identified targets were in ribosomal proteins (RL7a and RL10), SMC3, SAHH2, CLP1, heat shock proteins (HS90A and 90B), HDAC1, SIL1, and DHX40. These proteins have not previously been recognized as targets of staurosporine, which suggests that they may be off-target binding sites. There was no sequence similarity among the probe-binding region of these proteins, but this might be due to the wide selectivity of staurosporine. We also performed selectivity profiling of (*S*)-crizotinib, which was recently reported as an inhibitor of 7,8-dihydro-8-oxoguanine triphosphatase, MTH1.[22] As shown in Figure 7, MTH1 (8ODP) was identified as a target of (*S*)-crizotinib in our assay system. The identified site (K79) is located in a region that is critical for the protein activity of MTH1.[23] In addition to MET and MAP3K1, which are known targets of crizotinib, pseudokinase MLKL (mixed lineage kinase domain-like) was also identified as a target candidate. Two lysines (K230 and K331) on MLKL identified in our study were recently shown to be involved in ATP binding.[24] Therefore, this suggests that (*S*)-crizotinib and ATP compete for the ATP-binding region of MLKL. We also performed quenching experiments using 1 mM

dx.doi.org/10.1021/pr500845u | *J. Proteome Res.* 2014, 13, 5461–5470

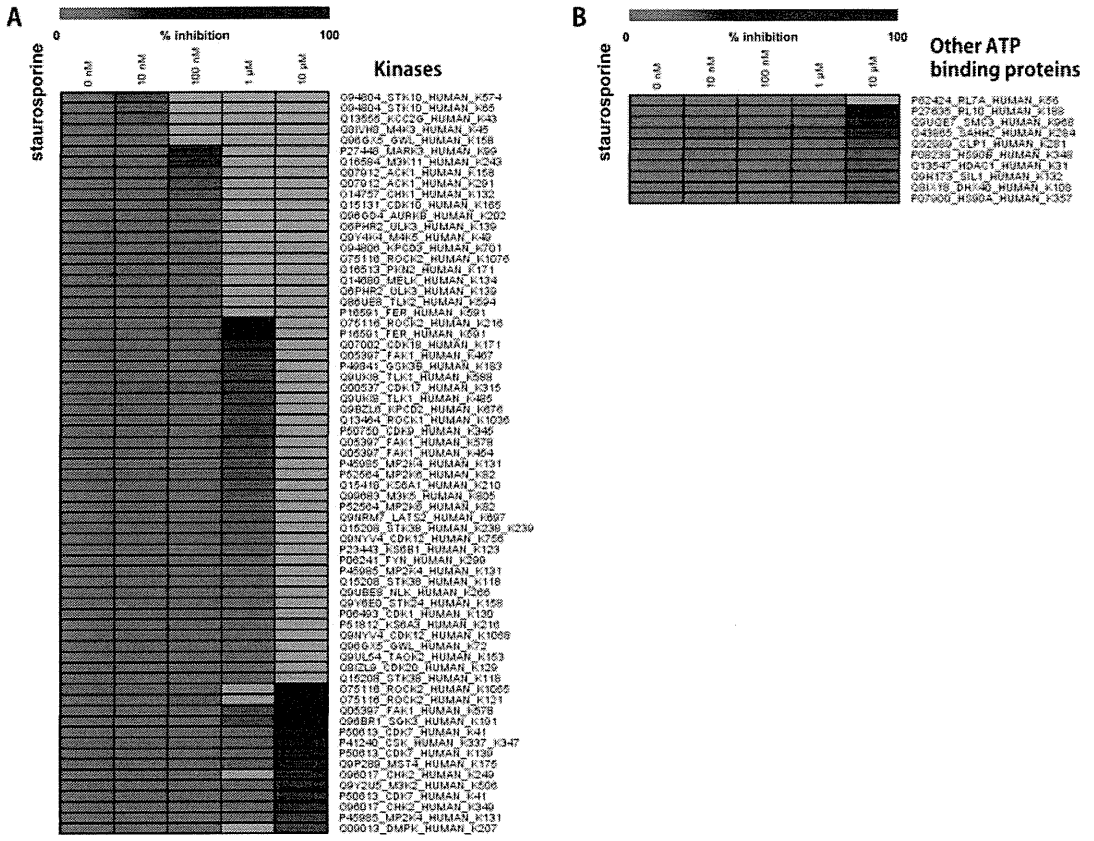

Figure 6. Heat map of staurosporine inhibition on kinases (A) and other ATP-binding proteins (B) in HeLa-S3 lysate.

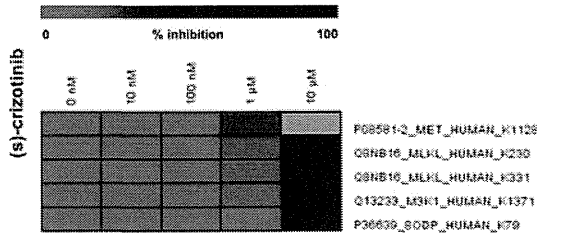

Figure 7. Heat map of (*S*)-crizotinib inhibition on kinases and other ATP-binding proteins in HeLa-S3 lysate.

lysine as a quencher. As shown in Supporting Information Figure 4, inhibition profiles of (*S*)-crizotinib were similar in experiments with and without quenching. This result confirms that the original protocol without quenching[7b] is useful for selectivity profiling.

In silico off-target profiling is a rapidly developing area.[25] In a large-scale study based on structural similarity to predict the off-target activity of 656 marketed drugs against 73 protein targets, about 50% of the predictions were confirmed experimentally.[25b] The relationship between off-target binding and side effects is also relevant for prediction of drug side effects.[26] These data suggest the importance of drug−protein interactions for in silico prediction of off-target binding and side effects. The off-target profiling method established in this study will complement in silico profiling due to the scalability, throughput, rigor, and high-confidence level of our system. Our approach can be used for basic data acquisition and validation of predicted results in silico. Thus, we believe off-target profiling using an acyl-ATP probe will become an important tool for avoidance of side effects in early drug discovery.

CONCLUSIONS

It is indispensable to distinguish specific targets from nonspecific targets in ATP-binding proteome analysis using a chemical proteomics approach. Here, we introduced an ATP competition assay to eliminate nonspecific targets and used high-resolution MS and MS/MS for accurate site identification of target lysine residues to create a rigorous ATPome list. This approach led to the identification of 539 ATP-binding protein candidates that included 178 previously unrecognized proteins, including ribosomal proteins. These findings indicate that the biological roles of ATP−-protein interactions might be more diverse than expected. Our ATPome data will contribute to decoding and understanding dynamic ATP−protein interactions on a systems level. We also proved the concept by expanding the targets of selectivity profiling of kinase inhibitors using the ATPome data set. This concept should also be applicable to other ATP-competitive kinase inhibitors to identify off-target interactions and understand the mechanisms of their side effects.

ASSOCIATED CONTENT

Supporting Information

Figure S1: Precision of label-free peptide quantification. Figure S2. Heat map of ATP competition on ribosomal proteins in HeLa-S3 lysate. Figure S3: Precision of spike-in SILAC peptide quantification. Figure S4: Effect of quenching after probe labeling on selectivity profiling of (*S*)-crizotinib. Table S1: Identified protein groups, peptides, and labeled sites by ATP-probe. This

material is available free of charge via the Internet at http://pubs.acs.org. The mass spectrometry proteomics data have been deposited to the ProteomeXchange Consortium (http://proteomecentral.proteomexchange.org) via the PRIDE partner repository with the data set identifier PXD001200.

AUTHOR INFORMATION

Corresponding Authors

*(J.A.) E-mail: jun_adachi@nibio.go.jp. Tel: +81-72-641-9862. Fax: +81-72-641-9861.

*(T.T.) E-mail: tomonaga@nibio.go.jp.

Notes

The authors declare no competing financial interest.

ACKNOWLEDGMENTS

This work was supported by Grants-in-Aid, Research on Biological Markers for New Drug Development H20-0005 to K.Y., from the Ministry of Health, Labour, and Welfare of Japan. This work was supported by Grants-in-Aid 25290054 to T.T. and 24681009 and 26640098 to J.A. from the Ministry of Education, Science, Sports, and Culture of Japan. We thank Daisuke Higo for advice on mass spectrum analysis.

REFERENCES

(1) Knowles, J. R. Enzyme-catalyzed phosphoryl transfer reactions. *Ann. Rev. Biochem.* **1980**, *49*, 877–919.

(2) (a) Walker, J. E.; Saraste, M.; Runswick, M. J.; Gay, N. J. Distantly related sequences in the alpha- and beta-subunits of ATP synthase, myosin, kinases and other ATP-requiring enzymes and a common nucleotide binding fold. *EMBO J.* **1982**, *1*, 945–51. (b) Saraste, M.; Sibbald, P. R.; Wittinghofer, A. The P-loop–a common motif in ATP- and GTP-binding proteins. *Trends Biochem. Sci.* **1990**, *15*, 430–4.

(3) (a) Berglund, O.; Eckstein, F. Synthesis of ATP- and dATP-substituted sepharoses and their application in the purification of phage-T4-induced ribonucleotide reductase. *FEBS J.* **1972**, *28*, 492–6. (b) Ito, J.; Heazlewood, J. L.; Millar, A. H. Analysis of the soluble ATP-binding proteome of plant mitochondria identifies new proteins and nucleotide triphosphate interactions within the matrix. *J. Proteome Res.* **2006**, *5*, 3459–69. (c) Graves, P. R.; Kwiek, J. J.; Fadden, P.; Ray, R.; Hardeman, K.; Coley, A. M.; Foley, M.; Haystead, T. A. Discovery of novel targets of quinoline drugs in the human purine binding proteome. *Mol. Pharmacol.* **2002**, *62*, 1364–72.

(4) (a) Daub, H.; Olsen, J. V.; Bairlein, M.; Gnad, F.; Oppermann, F. S.; Korner, R.; Greff, Z.; Keri, G.; Stemmann, O.; Mann, M. Kinase-selective enrichment enables quantitative phosphoproteomics of the kinome across the cell cycle. *Mol. Cell* **2008**, *31*, 438–48. (b) Bantscheff, M.; Eberhard, D.; Abraham, Y.; Bastuck, S.; Boesche, M.; Hobson, S.; Mathieson, T.; Perrin, J.; Raida, M.; Rau, C.; Reader, V.; Sweetman, G.; Bauer, A.; Bouwmeester, T.; Hopf, C.; Kruse, U.; Neubauer, G.; Ramsden, N.; Rick, J.; Kuster, B.; Drewes, G. Quantitative chemical proteomics reveals mechanisms of action of clinical ABL kinase inhibitors. *Nat. Biotechnol.* **2007**, *25*, 1035–44.

(5) (a) Qiu, H.; Wang, Y. Probing adenosine nucleotide-binding proteins with an affinity-labeled nucleotide probe and mass spectrometry. *Anal. Chem.* **2007**, *79*, 5547–56. (b) Patricelli, M. P.; Szardenings, A. K.; Liyanage, M.; Nomanbhoy, T. K.; Wu, M.; Weissig, H.; Aban, A.; Chun, D.; Tanner, S.; Kozarich, J. W. Functional interrogation of the kinome using nucleotide acyl phosphates. *Biochemistry* **2007**, *46*, 350–8.

(6) Chene, P. ATPases as drug targets: learning from their structure. *Nat. Rev. Drug Discovery* **2002**, *1*, 665–73.

(7) (a) Xiao, Y.; Guo, L.; Wang, Y.; Isotope-Coded, A. T. P. Probe for quantitative affinity profiling of ATP-binding proteins. *Anal. Chem.* **2013**, *85*, 7478–86. (b) Patricelli, M. P.; Nomanbhoy, T. K.; Wu, J.; Brown, H.; Zhou, D.; Zhang, J.; Jagannathan, S.; Aban, A.; Okerberg, E.; Herring, C.; Nordin, B.; Weissig, H.; Yang, Q.; Lee, J. D.; Gray, N. S.; Kozarich, J. W. In situ kinase profiling reveals functionally relevant properties of native kinases. *Chem. Biol.* **2011**, *18*, 699–710. (c) Lemeer, S.; Zorgiebel, C.; Ruprecht, B.; Kohl, K.; Kuster, B. Comparing immobilized kinase inhibitors and covalent ATP probes for proteomic profiling of kinase expression and drug selectivity. *J. Proteome Res.* **2013**, *12*, 1723–31. (d) Xiao, Y.; Guo, L.; Wang, Y. A targeted quantitative proteomics strategy for global kinome profiling of cancer cells and tissues. *Mol. Cell. Proteomics* **2014**, *13*, 1065–75.

(8) (a) Xiao, Y.; Guo, L.; Jiang, X.; Wang, Y. Proteome-wide discovery and characterizations of nucleotide-binding proteins with affinity-labeled chemical probes. *Anal. Chem.* **2013**, *85*, 3198–206. (b) Villamor, J. G.; Kaschani, F.; Colby, T.; Oeljeklaus, J.; Zhao, D.; Kaiser, M.; Patricelli, M. P.; van der Hoorn, R. A. Profiling protein kinases and other ATP binding proteins in *Arabidopsis* using acyl-ATP probes. *Mol. Cell. Proteomics* **2013**, *12*, 2481–96. (c) Wolfe, L. M.; Veeraraghavan, U.; Idicula-Thomas, S.; Schurer, S.; Wennerberg, K.; Reynolds, R.; Besra, G. S.; Dobos, K. M. A chemical proteomics approach to profiling the ATP-binding proteome of *Mycobacterium tuberculosis*. *Mol. Cell. Proteomics* **2013**, *12*, 1644–60.

(9) (a) Anastassiadis, T.; Deacon, S. W.; Devarajan, K.; Ma, H.; Peterson, J. R. Comprehensive assay of kinase catalytic activity reveals features of kinase inhibitor selectivity. *Nat. Biotechnol.* **2011**, *29*, 1039–45. (b) Davis, M. I.; Hunt, J. P.; Herrgard, S.; Ciceri, P.; Wodicka, L. M.; Pallares, G.; Hocker, M.; Treiber, D. K.; Zarrinkar, P. P. Comprehensive analysis of kinase inhibitor selectivity. *Nat. Biotechnol.* **2011**, *29*, 1046–51.

(10) Bilodeau, M. T.; Balitza, A. E.; Koester, T. J.; Manley, P. J.; Rodman, L. D.; Buser-Doepner, C.; Coll, K. E.; Fernandes, C.; Gibbs, J. B.; Heimbrook, D. C.; Huckle, W. R.; Kohl, N.; Lynch, J. J.; Mao, X.; McFall, R. C.; McLoughlin, D.; Miller-Stein, C. M.; Rickert, K. W.; Sepp-Lorenzino, L.; Shipman, J. M.; Subramanian, R.; Thomas, K. A.; Wong, B. K.; Yu, S.; Hartman, G. D. Potent *N*-(1,3-thiazol-2-yl)pyridin-2-amine vascular endothelial growth factor receptor tyrosine kinase inhibitors with excellent pharmacokinetics and low affinity for the hERG ion channel. *J. Med. Chem.* **2004**, *47*, 6363–72.

(11) Ong, S. E.; Blagoev, B.; Kratchmarova, I.; Kristensen, D. B.; Steen, H.; Pandey, A.; Mann, M. Stable isotope labeling by amino acids in cell culture, SILAC, as a simple and accurate approach to expression proteomics. *Mol. Cell. Proteomics* **2002**, *1*, 376–86.

(12) Rappsilber, J.; Mann, M.; Ishihama, Y. Protocol for micro-purification, enrichment, pre-fractionation and storage of peptides for proteomics using StageTips. *Nat. Protoc.* **2007**, *2*, 1896–906.

(13) Cox, J.; Neuhauser, N.; Michalski, A.; Scheltema, R. A.; Olsen, J. V.; Mann, M. Andromeda: a peptide search engine integrated into the MaxQuant environment. *J. Proteome Res.* **2011**, *10*, 1794–805.

(14) Nagaraj, N.; D'Souza, R. C.; Cox, J.; Olsen, J. V.; Mann, M. Feasibility of large-scale phosphoproteomics with higher energy collisional dissociation fragmentation. *J. Proteome Res.* **2010**, *9*, 6786–94.

(15) Gallien, S.; Duriez, E.; Crone, C.; Kellmann, M.; Moehring, T.; Domon, B. Targeted proteomic quantification on quadrupole-orbitrap mass spectrometer. *Mol. Cell. Proteomics* **2012**, *11*, 1709–23.

(16) Geiger, T.; Wehner, A.; Schaab, C.; Cox, J.; Mann, M. Comparative proteomic analysis of eleven common cell lines reveals ubiquitous but varying expression of most proteins. *Mol. Cell. Proteomics* **2012**, *11*, M111.014050.

(17) Buttgereit, F.; Brand, M. D. A hierarchy of ATP-consuming processes in mammalian cells. *Biochem. J.* **1995**, *312*, 163–7.

(18) Schwartz, D.; Gygi, S. P. An iterative statistical approach to the identification of protein phosphorylation motifs from large-scale data sets. *Nat. Biotechnol.* **2005**, *23*, 1391–8.

(19) McAllister, F. E.; Niepel, M.; Haas, W.; Huttlin, E.; Sorger, P. K.; Gygi, S. P. Mass spectrometry based method to increase throughput for kinome analyses using ATP probes. *Anal. Chem.* **2013**, *85*, 4666–74.

(20) Geiger, T.; Cox, J.; Ostasiewicz, P.; Wisniewski, J. R.; Mann, M. Super-SILAC mix for quantitative proteomics of human tumor tissue. *Nat. Methods* **2010**, *7*, 383–5.

(21) Karaman, M. W.; Herrgard, S.; Treiber, D. K.; Gallant, P.; Atteridge, C. E.; Campbell, B. T.; Chan, K. W.; Ciceri, P.; Davis, M. I.; Edeen, P. T.; Faraoni, R.; Floyd, M.; Hunt, J. P.; Lockhart, D. J.; Milanov,

Z. V.; Morrison, M. J.; Pallares, G.; Patel, H. K.; Pritchard, S.; Wodicka, L. M.; Zarrinkar, P. P. A quantitative analysis of kinase inhibitor selectivity. *Nat. Biotechnol.* **2008**, *26*, 127−32.

(22) Huber, K. V.; Salah, E.; Radic, B.; Gridling, M.; Elkins, J. M.; Stukalov, A.; Jemth, A. S.; Gokturk, C.; Sanjiv, K.; Stromberg, K.; Pham, T.; Berglund, U. W.; Colinge, J.; Bennett, K. L.; Loizou, J. I.; Helleday, T.; Knapp, S.; Superti-Furga, G. Stereospecific targeting of MTH1 by (*S*)-crizotinib as an anticancer strategy. *Nature* **2014**, *508*, 222−7.

(23) Fujii, Y.; Shimokawa, H.; Sekiguchi, M.; Nakabeppu, Y. Functional significance of the conserved residues for the 23-residue module among MTH1 and MutT family proteins. *J. Biol. Chem.* **1999**, *274*, 38251−9.

(24) Murphy, J. M.; Lucet, I. S.; Hildebrand, J. M.; Tanzer, M. C.; Young, S. N.; Sharma, P.; Lessene, G.; Alexander, W. S.; Babon, J. J.; Silke, J.; Czabotar, P. E. Insights into the evolution of divergent nucleotide-binding mechanisms among pseudokinases revealed by crystal structures of human and mouse MLKL. *Biochem. J.* **2014**, *457*, 369−77.

(25) (a) Keiser, M. J.; Setola, V.; Irwin, J. J.; Laggner, C.; Abbas, A. I.; Hufeisen, S. J.; Jensen, N. H.; Kuijer, M. B.; Matos, R. C.; Tran, T. B.; Whaley, R.; Glennon, R. A.; Hert, J.; Thomas, K. L.; Edwards, D. D.; Shoichet, B. K.; Roth, B. L. Predicting new molecular targets for known drugs. *Nature* **2009**, *462*, 175−81. (b) Lounkine, E.; Keiser, M. J.; Whitebread, S.; Mikhailov, D.; Hamon, J.; Jenkins, J. L.; Lavan, P.; Weber, E.; Doak, A. K.; Cote, S.; Shoichet, B. K.; Urban, L. Large-scale prediction and testing of drug activity on side-effect targets. *Nature* **2012**, *486*, 361−7. (c) Campillos, M.; Kuhn, M.; Gavin, A. C.; Jensen, L. J.; Bork, P. Drug target identification using side-effect similarity. *Science* **2008**, *321*, 263−6.

(26) Kuhn, M.; Al Banchaabouchi, M.; Campillos, M.; Jensen, L. J.; Gross, C.; Gavin, A. C.; Bork, P. Systematic identification of proteins that elicit drug side effects. *Mol. Syst. Biol.* **2013**, *9*, 663.

Oncogene (2014), 1–13

www.nature.com/onc

ORIGINAL ARTICLE

Nuclear accumulation of annexin A2 contributes to chromosomal instability by coilin-mediated centromere damage

T Kazami[1], H Nie[1], M Satoh[1], T Kuga[2], K Matsushita[1], N Kawasaki[1,2], T Tomonaga[1,2] and F Nomura[1]

Most human cancers show chromosomal instability (CIN), but the precise mechanisms remain uncertain. Annexin A2 is frequently overexpressed in human cancers, and its relationship to tumorigenesis is poorly understood. We found that annexin A2 is overexpressed in the nuclei of CIN cells compared with cells with microsatellite instability (MIN). Ectopic annexin A2 expression in MIN cells results in a high level of aneuploidy and induces lagging chromosomes; suppression of annexin A2 in CIN cells reduces such CIN signatures with apoptosis of highly aneuploid cells. Ectopic expression of annexin A2 in MIN cells reduces the expression of centromere proteins. Conversely, annexin A2-knockdown in CIN cells increases the expression of centromere proteins. Moreover, the endogenous expression levels of centromere proteins in CIN cells were greatly reduced compared with MIN cell lines. The reduced expression of centromere proteins likely occurred due to aberrant centromere localization of coilin, a major component of the Cajal bodies. These results suggest that nuclear accumulation of annexin A2 has a crucial role in CIN by disrupting centromere function.

Oncogene advance online publication, 27 October 2014; doi:10.1038/onc.2014.345

INTRODUCTION

Aneuploidy resulting from chromosomal instability (CIN) is a hallmark of human cancer. CIN is characterized by gains or losses of whole or large portions of chromosomes caused by continuous chromosome missegregation during mitosis. Another form of genetic instability, known as microsatellite instability (MIN), is characterized by mutation rates hundreds of fold higher than those of normal cells.[1,2]

The malfunction of a number of potential mitotic targets that may cause CIN has been identified, including overexpression or mutational inactivation of genes that regulate chromosome cohesion,[3–6] mutation of the spindle assembly checkpoint,[7,8] amplification of genes required for centrosome maturation[9–12] and mutational inactivation or aberrant expression of genes that regulate kinetochore-microtubule attachment dynamics.[13–20] We have recently reported that decreased expression of the nuclear membrane protein lamin B2 is involved in CIN.[21] However, alternative mechanisms of CIN remain to be uncovered.

Annexins are a family of cytosolic proteins that bind to membranes and are involved in a number of membrane-related processes.[22] Annexin A2 is also known to have a role in DNA synthesis and cell proliferation.[23,24] Moreover, annexin A2 is strongly expressed in several cancers,[25–27] although the precise mechanism through which overexpression contributes to tumorigenesis is poorly understood.

In this study, we performed a proteomic search to identify the factors involved in CIN by comparing the nuclear protein expression profiles of CIN and MIN colorectal cancer cell lines, and found that annexin A2 is significantly overexpressed in the nuclei of CIN cells. The involvement of annexin A2 in CIN was verified by the examination of chromosomal states upon ectopic expression of annexin A2 in diploid MIN cells or reduced expression of annexin A2 in CIN cells. Most strikingly, we showed evidence that reduced expression of core centromere proteins (CENPs), through aberrant centromere localization of coilin, is involved in CIN.

RESULTS

Proteomic analysis of differentially expressed nuclear proteins between CIN and MIN colorectal cancer cells

To improve the sensitivity and dynamic range of conventional two-dimensional (2D) gels, we used the agarose 2D-DIGE method to compare the protein expression profiles of CIN and MIN cell lines. On the basis of a previous study, colorectal cancer cell lines can be clearly segregated into two groups.[1] CIN cell lines show a dramatic variation in chromosome content among cells expanded through 20–30 generations, with the average difference from the modal chromosome number exceeding 20%; MIN cell lines, however, show minimal variation in chromosome content, with the average difference from the modal chromosome number being less than 8%.[1,28] Thus, we used HT29, SW480, SW837 and CaCO2 as CIN cell lines, and HCT116, RKO, DLD1 and SW48 as MIN cell lines. CIN reflects defects in mitotic processes, such as chromosome condensation, sister-chromatid cohesion, kinetochore structure and function, centrosome/microtubule formation and dynamics, as well as checkpoints. The factors responsible for these processes localize primarily in the nucleus; therefore, we decided to analyze nuclear proteins in CIN and MIN cell lines.

[1]Department of Molecular Diagnosis (F8), Graduate School of Medicine, Chiba University, Inohana, Chuo-ku, Chiba, Japan and [2]Laboratory of Proteome Research, National Institute of Biomedical Innovation, Saito-Asagi, Ibaraki City, Osaka, Japan. Correspondence: Professor T Tomonaga, Laboratory of Proteome Research, National Institute of Biomedical Innovation, 7-6-8 Saito-Asagi, Ibaraki City, Osaka 567-0085, Japan.
E-mail: tomonaga@nibio.go.jp
Received 27 February 2014; revised 3 September 2014; accepted 4 September 2014

Nuclei were isolated and nuclear proteins were extracted from each cell line. The nuclear extracts of each cell line were labeled with Cy5 for CIN cells and Cy3 for MIN cells. An internal standard, created by pooling aliquots of all samples, was labeled with Cy2. Next, 50-μg aliquots of each labeled protein sample were mixed and separated using agarose 2D-DIGE. To identify the differentially expressed nuclear proteins across the two groups of cell lines, four pair-wise comparisons were carried out between the representative CIN and MIN cell lines and then statistical analysis was performed across the four pairs.

Protein spots from CIN nuclei that showed increased or decreased expression were displayed as red or green, respectively (Figure 1a). The fluorescence volume of these spots was quantified using DeCyder imaging analysis software. Spots demonstrating a 1.5-fold increase or 1.5-fold decrease with a *P*-value $\leqslant 0.05$ were considered as having undergone a significant change in expression. We found that the expression of 42 proteins had increased and that of 64 proteins had decreased in CIN nuclei when compared with MIN nuclei. To identify the proteins, 500 μg of nonlabeled nuclear extract was separated by conventional agarose 2-DE, and proteins were visualized by Coomassie blue staining. We carefully compared the DIGE image with Coomassie blue-stained gels and picked 27 visible protein spots manually. Using mass spectrometry, a total of 15 proteins were identified (Figure 1, Supplementary Table S2). Annexin A2 shows increased expression in several types of cancer, and correlation of ANXA2 expression with tumor progression, recurrence and prognosis has also been reported,[27] although the precise mechanism of involvement of annexin A2 in tumorigenesis remains to be elucidated. Thus, we focused on annexin A2 for further investigation.

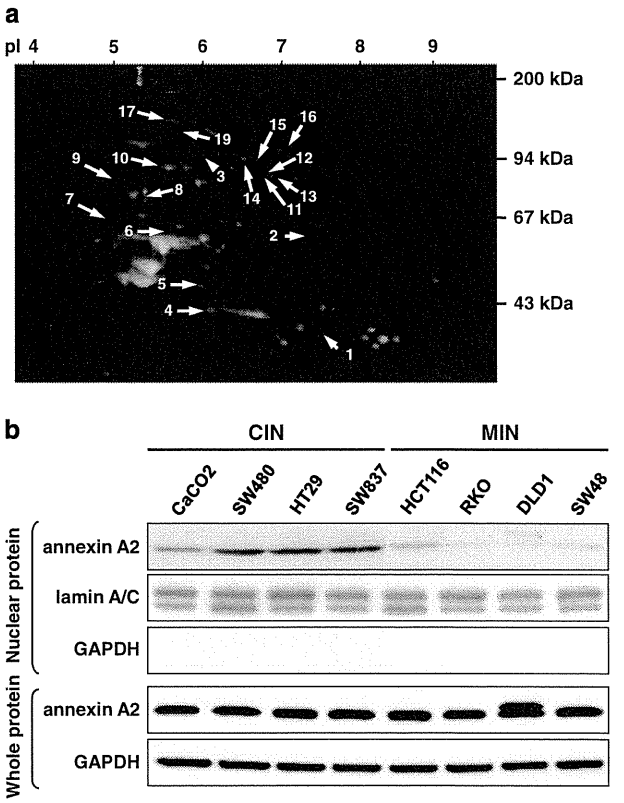

Figure 1. The amount of nuclear annexin A2 is increased in CIN cells. (**a**) Proteomic analysis of CIN (SW837) and MIN (DLD1) cell lines was performed using agarose 2D-DIGE. Nuclear extracts (NE) from each cell line were prepared and applied to 2D-DIGE as described in Supplementary Materials and Methods. Arrows indicate protein spots with increased (red) or decreased (green) intensities in CIN cells, and numbers correspond to the numbers in Supplementary Figure S1. (**b**) Western blot analysis of nuclear and whole cell extracts from CIN and MIN cells. Annexin A2 protein levels in the nuclei and whole cells were examined by western blotting using an anti-annexin A2 antibody. The purity of nuclear extracts and the equality of loading in each lane were confirmed by western blotting with anti-lamin A/C and -GAPDH antibodies. Nuclear (20 μg) and whole cell extracts (5 μg) were loaded and separated by electrophoresis on 10–20% gradient gels. Anti-annexin A2 antibody diluted 1:1000, anti-lamin A/C antibody diluted 1:250, anti-GAPDH antibody diluted 1:100 000 were used as primary antibodies. Rabbit anti-mouse IgG HRP diluted 1:1000, donkey anti-rabbit IgG HRP diluted 1:3000 in blocking buffer were used as secondary antibodies. Antigens on the membrane were detected by enhanced chemiluminescence detection reagents (see Materials and methods). The amount of annexin A2 protein was significantly higher in the nuclei of CIN cells, whereas there were no differences in the annexin A2 protein levels in CIN- and MIN-cell whole cell extracts. The additional annexin A2 band in DLD1 cells probably corresponds to an isoform of annexin A2.

The amount of annexin A2 was elevated in the nuclei of CIN cells vs MIN cells

Western blot analyses were performed to validate the differential expression of several proteins. The purity of nuclear extracts was confirmed by western blot analysis of the nuclear marker protein lamin A/C and the cytosolic protein GAPDH (Figure 1b, upper). Annexin A2 protein levels were higher in the nuclei of CIN cells as compared with MIN cells (Figure 1b, upper, Supplementary Figure S1a). In contrast, there were no differences in annexin A2 protein levels in CIN- and MIN-cell whole cell extracts (Figure 1b, lower).

Since annexin A2 contains an NES sequence and is actively transported to the cytoplasm,[29] the amount of nuclear annexin A2 is very low. The minute nuclear annexin A2 protein level was verified by western blotting using the same amounts of whole cell extracts and nuclear extracts loaded side by side (Supplementary Figure S1b). Note that 25% of the nuclear extract as compared with the blot shown in Figure 1b was loaded; consequently, no bands can be visualized.

Immunostaining showed that annexin A2 localizes uniformly in CIN cells, whereas it mainly localizes in the cytoplasm of MIN cells (Figures 2a and c). To clearly verify the difference in the amount of nuclear annexin A2 between CIN and MIN cells, immunostaining of annexin A2 was performed using the nuclear export inhibitor leptomycin B. The localization of annexin A2 clearly shifted from the cytoplasm to the nucleus by leptomycin B treatment (Figure 2b), and the nuclear intensity of annexin A2 staining in leptomycin B-treated CIN cells was markedly higher than in MIN cells (Figures 2b and c). Thus, a small proportion of annexin A2 localizes to the nucleus, and nuclear localization is more pronounced in CIN cells than in MIN cells, but it is actively exported to the cytoplasm.

Ectopic nuclear expression of annexin A2 induces aneuploidy

The above observations raised the question of whether overexpression of annexin A2 in the nucleus induces the CIN phenotype. To answer this question, annexin A2-FLAG was transiently introduced into the MIN cell lines RKO and HCT116, followed by fluorescence *in situ* hybridization (FISH) analysis with CEP7, 8, 10, 12, 15 and 17 centromere probes, and immunostaining using anti-FLAG antibody. The expression level of FLAG-tagged annexin A2 was comparable with that of endogenous annexin A2 (Figure 3a). FISH analysis of the annexin A2-FLAG expressed in HCT116 and RKO cells at 72 h after transfection showed that many cells overexpressing annexin A2 have abnormal chromosome numbers (Figure 3b). The number of centromeric signals for chromosomes 7, 8, 10, 12, 15 and 17 were counted in at least 250 cells, and we found that 40–60% of

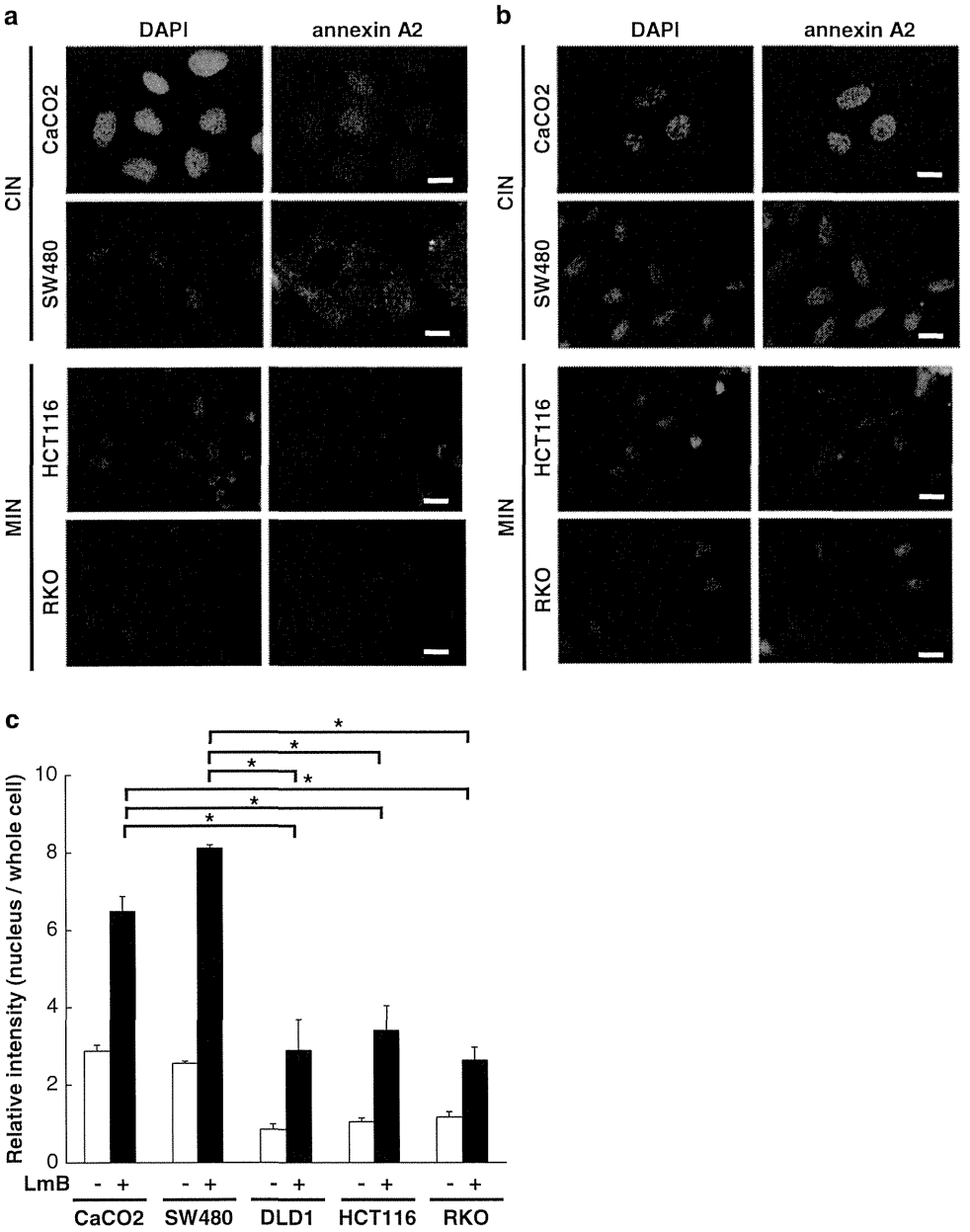

Figure 2. Annexin A2 is more abundant in the nuclei of CIN cells than MIN cells. (**a**) Immunostaining of annexin A2 in CIN and MIN cells. Annexin A2 localizes uniformly in CIN (CaCO2 and SW480) cells, whereas it mainly localizes in the cytoplasm of MIN (HCT116, and RKO) cells. (**b**) Immunostaining of annexin A2 in CIN and MIN cells treated with nuclear export inhibitor. Annexin A2 accumulated in the nucleus after leptomycin B treatment, and shows higher nuclear levels in CIN (CaCO2 and SW480) cells as compared with MIN (HCT116, and RKO) cells. CIN and MIN cell lines were incubated for 3 h in the presence of 200 nM leptomycin B followed by immunostaining with annexin A2 antibody. Cells were counterstained with DAPI (blue). (**c**) Relative intensity of annexin A2 between nuclei and whole cells in CIN and MIN cells with or without leptomycin B. Stained samples were viewed under an Axio Imager Z1 microscope, and the intensity of annexin A2 in the nucleus and whole cell was quantified using AxioVision software. The area of each cell was delimited and the pixel intensity was calculated. Relative intensities of annexin A2 between nuclei and whole cells are represented as means ± s.d. At least 100 cells were quantified. Bar, 10 μm. *$P \leqslant 0.05$ by Wilcoxon-Mann-Whitney test.

annexin A2-FLAG transfected RKO cells showed aneuploidy, as compared with about 5–15% of FLAG-only transfected control cells (Figure 3c). Aneuploid cells were also significantly increased in annexin A2-FLAG transfected HCT116 cells as compared with control cells (Supplementary Figure S2a). Moreover, the induction of aneuploidy was observed by overexpression of non-tagged annexin A2 (Supplementary Figure S2b), which indicates that FLAG-tagged annexin A2 is functional and supports our hypothesis that annexin A2 overexpression induces aneuploidy.

Transient ectopic nuclear expression of annexin A2 induces CIN

The term CIN refers to the accelerated rate of whole chromosomal gain and loss, but the term is often used in a more general sense to show a high level of aneuploidy with complex karyotypes.[2,30] Recently, the accelerated rate of aneuploidy was clearly shown by 'CIN analysis', which is the quantification of the modal chromosome number and the percentage of cells deviating from that mode in individual colonies grown from a single cell, either untreated or forced to recover from nocodazole- or

monastrol-induced mitotic delay for one or more consecutive days.[28] In this analysis, both MIN cells and CIN cells increase aneuploid cells immediately after nocodazole or monastrol treatment. However, the number of aneuploidy cells declines to basal level upon growth without further treatment in MIN cells, whereas aneuploidy persists in CIN cells, which acquired an ability to grow efficiently with nondiploid karyotypes. This persistence of aneuploidy after induction of chromosome missegregation is necessary for the CIN phenotype. Thus, we investigated if transiently overexpressed annexin A2 cells could maintain

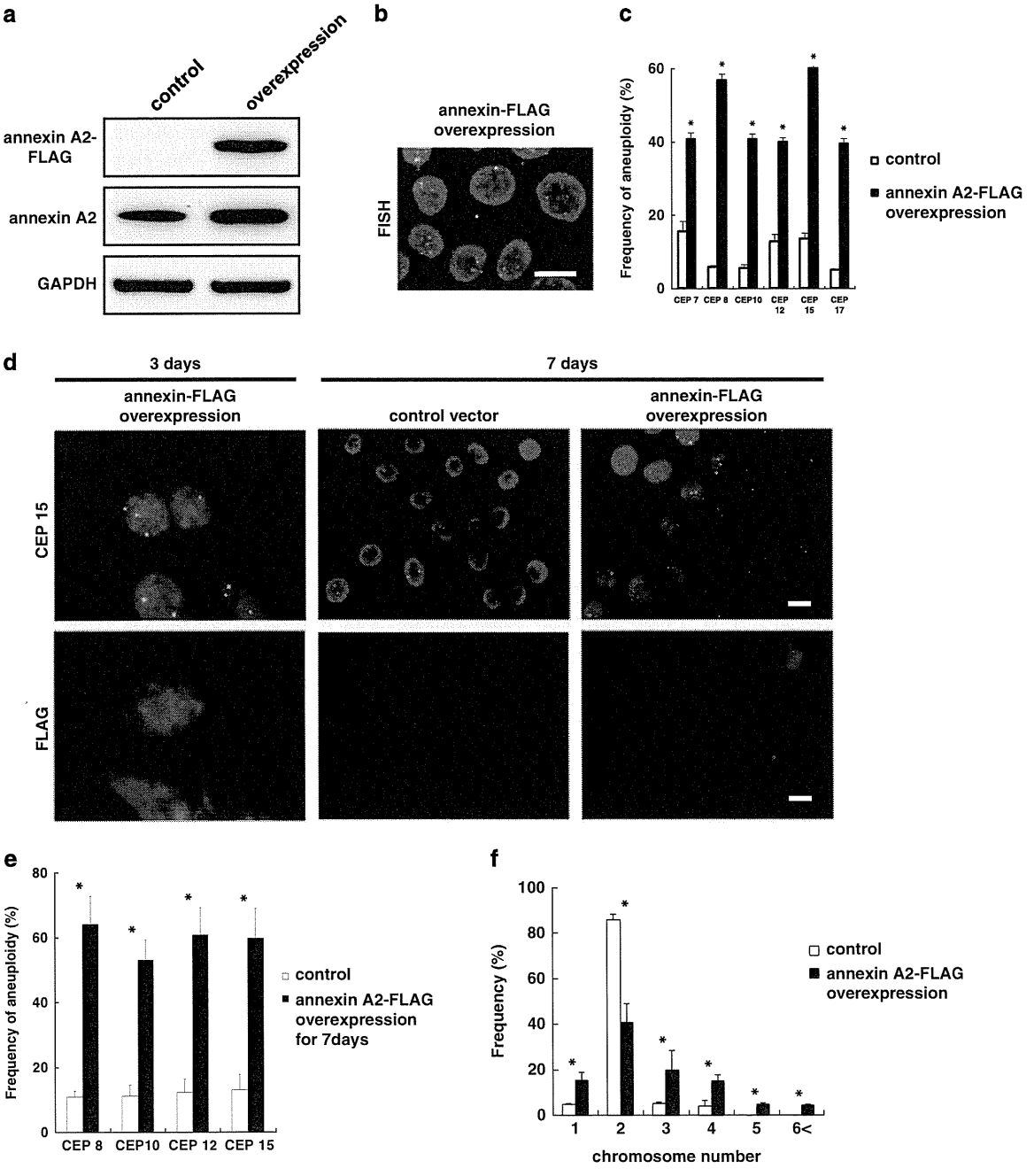

	total mitotic cell counted	frequency of lagging chromosome
control	262	3.4
annexin A2 overexpression for 72hrs	257	22.2
annexin A2 overexpression for 7 days	156	10.3

aneuploidy. We plated annexin A2-overexpressed cells at low density, grew them for 7 days until the cells formed individual colonies, and analyzed the chromosome number by FISH using CEP8, 10, 12 and 15 centromere probes. Examples of aneuploid cells grown for 3 and 7 days are shown in Figure 3d. As expected, annexin A2-overexpressed cells showed a high percentage of aneuploid cells even after 7 days in RKO (Figure 3e) and HCT116 cells (Supplementary Figure S2c), consisting of various chromosome numbers from one to more than six as compared with control cells (Figure 3f (CEP12); Supplementary Figure S2d (CEP15)). Furthermore, ectopic expression of annexin A2 markedly increased lagging chromosomes either 72 h or 7 days after transfection (Figure 3g), possibly due to merotelic microtubule-chromosome attachment, a leading cause of CIN. Note that aneuploidy and chromosome missegregation persists at least for 7 days when annexin A2 localizes mainly in cytoplasm (Figure 3d). These results suggest that transient ectopic nuclear expression of annexin A2 maintains aneuploidy and chromosome missegregation and also enables cells to grow efficiently with nondiploid karyotypes, which is a unique feature of CIN.

Knockdown of annexin A2 in CIN cells suppresses the CIN signature and induces apoptosis of highly aneuploid cells

If overexpression of annexin A2 is a critical step in the development of CIN, suppression of annexin A2 expression in CIN cell lines should repress the CIN phenotype. An example of suppression of CIN has previously been shown by overexpression of the kinesin-13 microtubule depolymerases MCAK and Kif2b by reducing kinetochore-microtubule attachment hyperstability that causes merotelic microtubule attachment.[17] Overexpression of each kinesin significantly suppresses the incidence of lagging chromosomes, chromosome missegregation rates and deviation from the modal chromosome number in CIN cell lines, and restores faithful chromosome segregation to cancer cells that otherwise shows CIN. As intercellular heterogeneity with respect to the chromosome copy number is a typical characteristic of CIN cell lines,[1,28] we examined whether suppression of annexin A2 expression reduces chromosome number heterogeneity.

CaCO2 cells were transfected with two different annexin A2 small interfering RNAs (siRNA-1, -2) or control siRNA, and chromosome numbers of single-cell colonies as described in the legend of Figure 3d were analyzed by FISH with CEP10 and CEP17 probes 7 days after transfection. Annexin A2 expression was greatly suppressed by the siRNAs (Figure 4a). As shown in Figure 4b (CEP17) and Supplementary Figure S3a (CEP10), CaCO2 cells exhibited marked heterogeneity in chromosome number. Strikingly, suppression of annexin A2 expression decreased the frequency of highly aneuploid cells, and as a result, reduced the intercellular heterogeneity of the chromosomes, and the distribution of the chromosome number shifted to the left (Figure 4b, Supplementary Figure S3a). The frequency of cells showing a less than modal chromosome number (four for chromosome 10 and five for chromosome 17) increased in annexin A2-knockdown CaCO2 cells (Figure 4c; Supplementary Figure S3b).

To investigate the mechanism of decreased high aneuploidy, we examined if suppression of annexin A2 reduces the missegregation rate of the chromosomes. To do this, the frequency of lagging chromosomes was examined in annexin A2-knockdown CIN cells. CaCO2 cells were transfected with annexin A2 siRNAs, and the number of lagging chromosomes was counted in at least 250 anaphase cells 72 h after transfection. As expected, reduced expression of annexin A2 in CaCO2 cells with siRNAs decreased the frequency of lagging chromosomes from 48.0 to 21.4% (Figure 4d).

Suppression of highly aneuploid cells might be also caused by apoptosis of the aneuploid cells. Thus, we tested if suppression of annexin A2 induces apoptosis of severely aneuploid cells. We examined the expression of two apoptotic markers, cleaved caspase 3 and cleaved PARP, in annexin A2-knockdown CaCO2 cells. Forty-eight hours after transfection of annexin A2 siRNAs, the expression of cleaved caspase 3 and of cleaved PARP greatly increased (Figure 4e). These observations suggested that annexin A2 overexpression increases CIN cell tolerance to chromosome gain. Thus, when annexin A2 is knocked down in CIN cells, cells that gain extra chromosomes may be eliminated via apoptosis, whereas cells losing chromosomes may survive. Decreased frequency of lagging chromosomes by annexin A2-knockdown might also contribute to the suppression of CIN signatures.

Nuclear annexin A2 interacts with coilin, a major component of Cajal bodies

To investigate how excess annexin A2 in the nucleus contributes to mitotic defects leading to CIN, we searched for proteins that interact with annexin A2 in the nucleus. RKO and HCT116 MIN cell lines that stably express annexin A2-FLAG were treated with leptomycin B, and nuclear extracts were prepared and immunoprecipitated with magnetic beads coupled with anti-FLAG antibody. Immunoprecipitated proteins were separated by SDS–polyacrylamide gel electrophoresis and comprehensively identified using mass spectrometry (Supplementary Table S3). Among the proteins we identified, coilin has recently been reported to be involved in a cell response triggered by centromere structure instability and mitotic defects.[31] Coilin is a major component of Cajal bodies (CBs),[32] and recent studies have shown that when cells are infected with herpes simplex virus type 1, CBs disassemble and coilin accumulates at the damaged centromere to interact with centromeric DNA.[31] Thus, we sought to determine whether annexin A2 overexpression affects the function of coilin, CBs and centromeres.

Ectopic expression of annexin A2 in MIN cells induces scattering and colocalization of coilin with centromeres, whereas annexin A2-knockdown in CIN cells converges scattered coilin

First, the interaction between annexin A2 and coilin was confirmed by immunoprecipitation of annexin A2-FLAG, followed

Figure 3. Overexpression of annexin A2 induces aneuploidy in cells of the MIN RKO line. (**a**) An annexin A2-FLAG expression plasmid was transfected into RKO cells, and the expression of annexin A2-FLAG was assessed by western blotting using an anti-FLAG antibody after 72 h. Lane 1: control; lane 2: annexin A2-FLAG-transfected RKO cells. (**b**) Analysis of chromosome numbers in annexin A2-overexpressed MIN cells. RKO cells were transfected with an annexin A2-FLAG expression plasmid, and FISH analysis was performed using centromere probes (CEP7: green, 12: red). (**c**) Frequency of aneuploidy (the deviation from diploid) in RKO cells overexpressing annexin A2-FLAG 72 h after transfection. CEP7, 8, 10, 12, 15 and 17 signals were examined in at least 250 cells. (**d**) CIN analysis of annexin A2-overexpressed MIN cells. Annexin A2-FLAG-oxerexpressed RKO cells were plated at low density and colonies grown from single cells were fixed after 3 and 7 days. Individual colonies grown from a single cell were analyzed by FISH using the CEP15 probe (green). RKO cells show various chromosome numbers 7 days after transfection. (**e**) Frequency of aneuploidy (the deviation from diploid) in annexin A2-FLAG-overexpressed RKO single-cell colonies 7 days after transfection. CEP8, 10, 12 and 15 signals were examined in at least 250 cells. (**f**) Distribution of chromosome number in annexin A2-FLAG-overexpressed RKO single-cell colonies 7 days after transfection. Chromosome numbers of single-cell colonies were analyzed by FISH using the CEP12 probe after 7 days in at least 300 cells. Overexpression of annexin A2 increased the intercellular heterogeneity of the chromosome number. (**g**) Frequency of lagging chromosomes in annexin A2-FLAG-overexpressed RKO single-cell colonies 72 h and 7 days after transfection. Bar, 10 μm. *$P \leqslant 0.05$ by Wilcoxon-Mann-Whitney test.

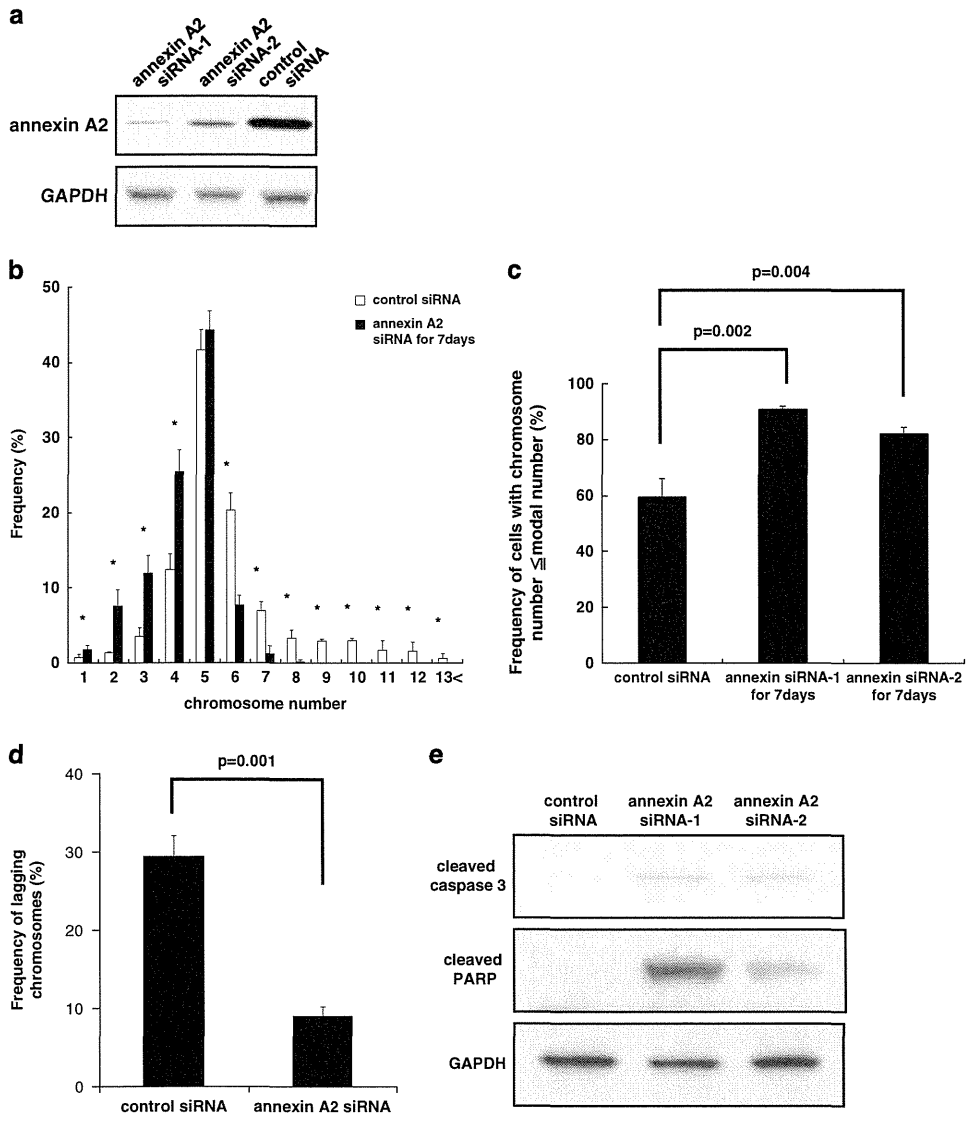

Figure 4. Suppression of annexin A2 reduces intercellular heterogeneity in the chromosome copy number associated with CIN. (**a**) Two different annexin A2 siRNAs, 1 and 2, were transfected into CaCO2 cells, and the expression of annexin A2 was assessed by western blotting after 72 h. (**b**) CIN analysis and distribution of chromosome number in annexin A2-knockdown CIN cells. Annexin A2-knockdown CaCO2 cells with siRNA 2 were plated at low density, and colonies grown from single cells were isolated. Chromosome numbers of single-cell colonies were analyzed by FISH using the CEP17 probe after 7 days in at least 300 cells. Suppression of annexin A2 expression reduced the intercellular heterogeneity of the chromosome number. (**c**) Frequency of cells exhibiting equal to or less than the modal chromosome number (chromosome 17) in annexin A2-knockdown CaCO2 cells. Centromere signals were counted in at least 300 cells. (**d**) Frequency of lagging chromosomes in annexin A2-knockdown CaCO2 single-cell colonies 72 h after transfection. At least 250 cells were counted. (**e**) Western blot analyses of apoptotic markers in annexin A2-knockdown CaCO2 cells. Western blot analyses were performed using anti-cleaved caspase 3 and cleaved PARP antibodies in control and annexin A2-suppressed CaCO2 cells 48 h after transfection. $^*P \leqslant 0.05$ by Wilcoxon–Mann–Whitney test.

by western blotting using an anti-coilin antibody (Supplementary Figure S4a). Next, we investigated the localization of coilin upon ectopic expression of annexin A2. HCT116 cells were transiently transfected with annexin A2-FLAG, and coilin was immunostained with a specific antibody 72 h after transfection (Figure 5a). Annexin A2-expressing cells were verified by immunostaining using an anti-FLAG antibody (Figure 5a). The percentage of HCT116 cells that overexpressed annexin A2-FLAG was 79.3–96.5%. Strikingly, scattered coilin staining was observed in the nuclei of annexin A2-FLAG-overexpressed HCT116 and DLD1 cells (Figure 5a, Supplementary Figure S4b), which contrasts markedly to the several large stained foci observed in the control cells. The frequency of cells containing $\geqslant 6$ foci significantly increased in annexin A2-FLAG-overexpressed cells as compared with control cells (Figure 5b). This indicates that overexpression of annexin A2 induces the disassembly of CB.

To examine if CIN cells that naturally accumulate annexin A2 in the nucleus show the same pattern of scattered coilin as in annexin A2-overexpressed MIN cells, we performed immunostaining of coilin in CaCO2 and SW480 cells. As expected, scattered coilin was observed in these cells (Figure 5a, Supplementary Figure S4b). Intriguingly, when the expression of annexin A2 in CaCO2 and SW480 cells was suppressed by siRNA, scattered coilin converged and several large foci were observed, as seen in MIN cells (Figure 5c, Supplementary Figure S4b). The frequency of cells containing $\geqslant 6$ foci was significantly lower in siRNA-treated cells as compared with control cells (Figure 5d, Supplementary Figure S4c).